Laser trimming of the operating wavelength of silicon nitride racetrack resonators

GRETA DE PAOLI[1,2,*], SENTA L. JANTZEN[2], THALIA DOMINGUEZ BUCIO[2], ILIAS SKANDALOS[2], CHRISTOPHER HOLMES[2], PETER G. R. SMITH[2], MILAN M. MILOSEVIC[2] AND FREDERIC Y. GARDES[2]

[1]*Department of Information Engineering, Università degli Studi di Padova, Via Giovanni Gradenigo 6, 35131, Padova, Italy*
[2]*Optoelectronics Research Centre, University of Southampton, Southampton SO17 1BJ, UK*
[*]*gdp1n18@soton.ac.uk*

Abstract: We demonstrate the possibility of post-fabrication trimming of the response of nitrogen-rich silicon nitride racetrack resonators by using an ultraviolet laser. The results revealed the possibility to efficiently tune the operating wavelength of fabricated racetrack resonators to any point within the full free spectral range. This process is much faster than similar, previously presented methods (in the order of seconds, compared to hours). This technique can also be applied to accurately trim the optical performance of any other silicon photonic device based on nitrogen-rich silicon nitride.

1. Introduction

Recently, the short-wave infrared spectral region (around 2 μm wavelength) has emerged as a promising candidate for the realisation of next-generation communication systems and sensors [1]. The extensive research in this area is driven by the fact that the hollow-core photonic bandgap optical fibres have low loss (0.1 dB/km) in the 1900 nm-2100 nm wavelength range (which is approximately 0.4 dB/km lower than the loss of conventional single-mode optical fibres) [2], while the optical gain window of thulium doped fibre amplifiers resides at around 1910 nm-2020 nm [3]. Additionally, such systems are compatible with silicon photonics technology, as the material loss of silicon dioxide is low at 2 μm [4, 5]. Low-loss waveguides, high-speed defect photodiodes (20 Gb/s at 2000 nm) and carrier depletion ring modulators (20 Gb/s at 1950 nm) have all been realized in the silicon-on-insulator (SOI) platform at short-wave infrared wavelengths [6–9].

The SOI platform has become mainstream in silicon photonics, however, silicon nitride (SiN) has emerged as an alternative, due to its promising optical properties. Silicon nitride is a CMOS compatible material which is transparent throughout most of the visible wavelength range (down to about 500 nm) where silicon is opaque [10]. This makes it suitable for silicon photonic applications below 1.1 μm, such as optical communications at 850 nm or therapeutic sensing in the visible wavelength range [11]. Similarly to SOI, the silicon nitride platform, with silicon dioxide cladding, also has negligible material absorption in the near- and mid-infrared spectral ranges up to the wavelength of 3.7 μm, where optical losses increase due to high material absorption in silicon-dioxide [10].

SiN also possesses manufacturing flexibility with a moderate refractive index contrast which can be conveniently tuned using different deposition techniques. It can be either deposited by Low Pressure Chemical Vapor Deposition (LPCVD) at high temperatures (>700 °C) or by Plasma Enhanced Chemical Vapour Deposition (PECVD) at low temperatures (<400 °C). The former method allows precise control over homogeneity and thickness, while the latter allows for the deposition of silicon-rich or nitrogen-rich layers by adjusting the silicon-nitrogen ratio [12–14]. For all these reasons, silicon nitride has been successfully used for realising low-loss waveguides (≈0.1 dB/m, orders of magnitude lower than SOI waveguides), wavelength multiplexers, interferometers, and optical filters [13, 15–17]. Additionally, two photon absorption of SiN is negligible in the telecom bands (1.5 - 1.6 μm and 1.9 - 2.1 μm), which makes it suitable for high frequency

combs and super-continuum generation in strip waveguides [18, 19].

Ring/racetrack resonators are fundamental components of silicon photonics circuits and systems. They are suitable for a variety of applications including optical filtering [20], switching, modulation [21], and sensing [22]. However, these devices are very prone to fabrication uncertainties and environmental changes. This is particularly pronounced in the SOI platform due to its high refractive index contrast and the high thermo-optic coefficient of silicon ($dn_{Si}/dT = 1.86 \times 10^{-4}$ K^{-1}). For example, a 1 nm variation in SOI waveguide width can cause a 1 nm shift in the operating wavelength, while the temperature sensitivity of the resonant wavelength peak typically varies between 60 pm/K and 100 pm/K [23, 24]. Therefore, both active device tuning, and various post-fabrication trimming techniques have been used to precisely control the resonant wavelength [25–28].

Thermo-optical [29] and electro-optical [21] effects can be used to tune the effective refractive index, but permanent trimming is usually required. Passive devices are also preferred due to the lower complexity and power consumption. This requirement is even more critical for more complex devices with multiple resonators, for example in channel dropping filters. In the SOI platform, a permanent change in the resonant wavelength can be obtained by post-fabrication ion implantation and selective laser annealing. These techniques have been proven successful for silicon ring resonators, however, it involves an additional fabrication step, which increases the costs, and requires precise control of the laser power used for annealing [25, 30]. Another technique involves the deposition of a photosensitive polymer layer on top of the waveguides. The polymer is subsequently exposed to laser radiation [31–33]. This method can be applied to silicon and silicon nitride resonators, but it lacks CMOS compatibility, and requires an additional deposition step.

The refractive index of silicon oxide, silicon nitride and silicon oxynitride can also be modified by either e-beam or UV irradiation [34–36]. Haeiwa *et al.* presented a method for permanently tuning the resonant wavelength of vertically coupled silicon nitride microring resonators by UV irradiation. They obtained a resonant wavelength shift of -12.1 nm exposing the whole ring for 24 hours. This technique is similar to the one proposed here. However, the method proposed in this paper utilises a laser spot size of 7 μm, which allows to reduce the exposure time to a few seconds. This technique is, therefore, suitable for an inline trimming process as the devices can potentially be trimmed and monitored in real time.

2. Design and fabrication

The resonant wavelength shift in a ring/racetrack resonator depends on the mode effective index and the optical path length at the wavelength of interest. The mode effective index at a given temperature depends on the material refractive index, waveguide dimensions, and operating wavelength. We have used Lumerical Mode Solutions for simulation analysis, assuming the refractive index of 1.9 for the N rich silicon nitride material [13].

Rib waveguides with 1 μm height, 200 nm slab layer, and a 3 μm buried oxide layer have been used. Using 1 μm wide waveguides, we have designed and fabricated racetrack resonators with 50 μm radius, coupling length of 10 μm and an edge-to-edge waveguide spacing of 600 nm. Both resonators with and without top oxide cladding have been simulated. According to our simulation analysis, a Q factor of 1700 and an extinction ratio of 25 dB were obtained for racetrack resonators with top oxide cladding, while the samples without oxide cladding experienced Q factor of 5000 and extinction ratio of 25 dB at 1950 nm wavelength.

Rib waveguides and racetrack resonators were fabricated on a nitrogen-rich silicon nitride layer, grown on a 200 mm Si wafer with a 3 μm thermally grown SiO$_2$. The SiN layer was deposited at 350 °C using NH$_3$-free PECVD, as described in [13]. The devices were patterned using deep ultraviolet lithography and inductively coupled plasma etching. A 1 μm thick layer of PECVD SiO$_2$ was finally deposited at 350 °C on top of some of the fabricated samples to serve

as cladding and to investigate the laser trimming technique with and without a top oxide cladding. The gratings used to provide coupling of light to and from the single-mode fibres used for testing, were optimised for TE polarisation. They were fabricated with a period of 1470 nm and a target duty cycle of 50%.
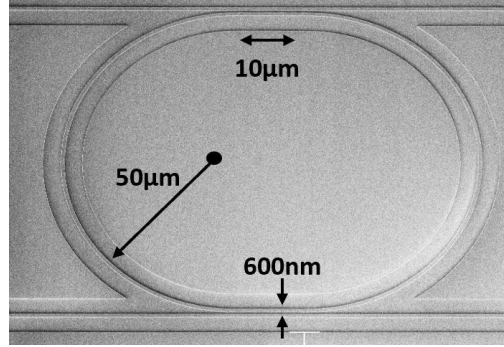

Fig. 1. SEM image of one of the resonators.

3. Experimental results

3.1. Setups and procedure

The measurements were performed using a TLK-L1950R tunable laser centred at 1950 nm (tuning range between 1890 and 2010 nm) and a PDA10DT-EC InGaAs photodetector (0.9 - 2.57 μm). The polarisation of the light launched into the devices was set using a polarisation controller to ensure that only TE modes were allowed to propagate. Similarly, the chips were placed on a thermal stage to control the effect of the temperature on the spectral response of the devices. The output voltage from the photodetector, which was connected to a fibre coupled to the through port of the resonator, was measured. This voltage was then converted into insertion loss, by comparing it to the voltage measured for a transmission through a straight waveguide of identical length.

A technique called Small Spot Direct Ultraviolet Writing (SSDUW), shown in Fig. 2 was used for the trimming experiments. This system is usually employed to write waveguides and Bragg gratings on chips and optical fibres [37, 38]. The devices were exposed to a 244 nm frequency-doubled continuous wave argon-ion laser. The light from the laser was split into two arms using a beam splitter, and recombined and focused into a 7 μm spot onto the sample surface. This focused Gaussian spot contained an interference pattern (as shown as side view in Fig. 2), which, in combination with the electro-optical modulator (EOM), can be used to create Bragg gratings [39]. For trimming, however, this feature is not desirable and the sample was continuously translated underneath the laser spot, blurring out the interference fringes. The laser output at the sample surface was 25 mW. The fluence was set to 40 kJ/cm^2.

The racetrack resonators were exposed as shown in Fig. 3. In this way, for each line, two arcs of 7 μm were exposed, achieving a total combined exposed length of 14 μm. This length is approximated, as it depends on the vertical position of the line and the profile of the laser beam. In order to characterise a dependence of the resonant wavelength shift on the exposed length, four lines were written on the same resonator. The racetrack resonators were characterised after each exposure.
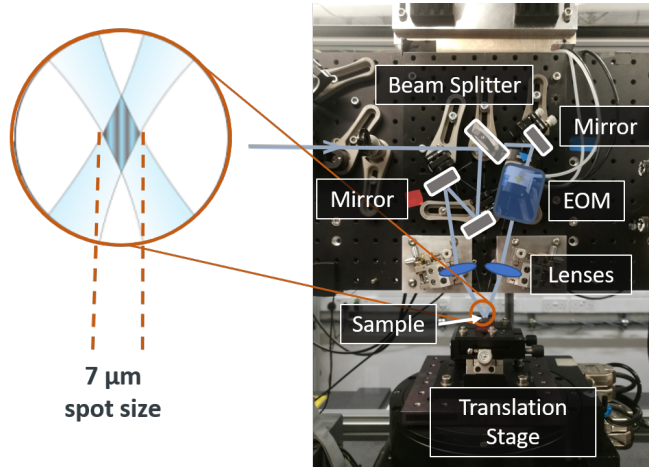
Fig. 2. Setup used for small spot direct UV writing in trimming experiments.
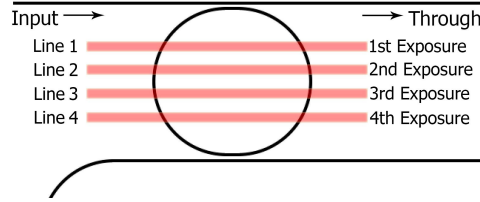

Fig. 3. Schematic of the device and the writing procedure.

3.2. Results

The transmission spectra of unexposed and exposed racetrack resonators (from 1 to 4 lines) are compared on Fig. 4 . As it can be seen, the resonant wavelength shift is observable in devices both with and without a top oxide cladding. The measurements were conducted with a 50 pm resolution. It was found that the shift in resonant wavelength peak was linearly dependent on the number of lines written across the resonator, and therefore, it is dependent on the length of the racetrack that has been exposed to the laser, as can be seen in Fig. 5. Due to an alignment error, the 4th line was closer to the straight section and the length of the exposed section could be slightly larger than for the other lines. From the linear dependence, it is possible to derive the minimum length that needs to be exposed in order to cover a full free spectral range (FSR) of 6.15 nm, which, in this case, is around 106 µm (corresponding to an exposure of 8 lines). A resonant wavelength shift of 6.95 nm has been experimentally observed exposing a total length of approximately 126 µm (9 lines, at a distance of one spot size to each other), demonstrating that it is possible to achieve this result; this implies that the device is completely tunable with the presented technique.

A simulation analysis has been carried out to quantify material's refractive index change (Fig. 6). The simulation did not focus on precisely obtaining the same group refractive index; instead, its aim was to match the shift of the resonant wavelength. The same shift as in the last exposure of 9 lines, was observed when, in the simulation, the refractive index of silicon nitride in the whole racetrack was changed by -7×10^{-3}, which corresponds to a change of -6×10^{-3} in the effective refractive index (Fig. 6b). Considering $\Delta n/n \propto L_{exp}/L_{tot}$ (where n is the refractive index, Δn is the change in the refractive index, L_{tot} is the total length of the resonator, and
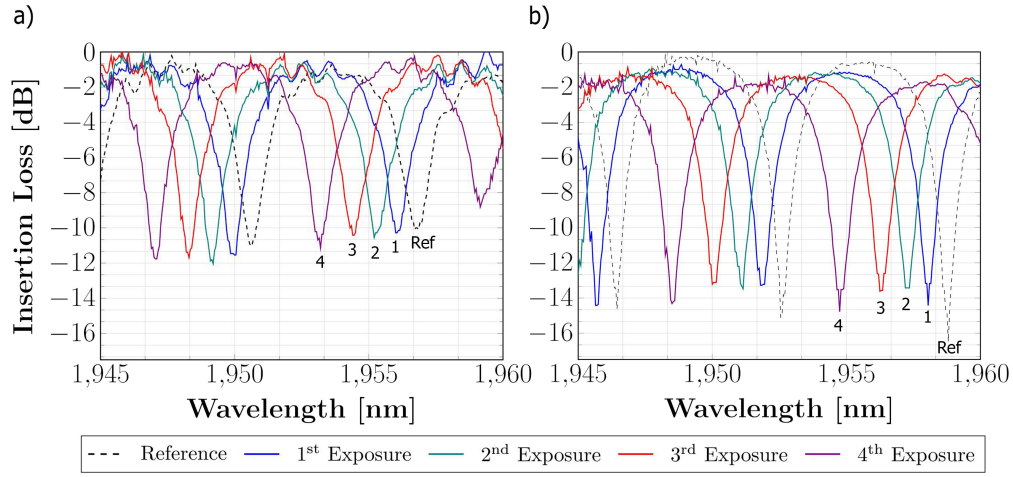
Fig. 4. Transmission spectra of fabricated racetrack resonators for different lengths of the exposed section of the resonator. a) Device without oxide cladding, b) device with oxide cladding.
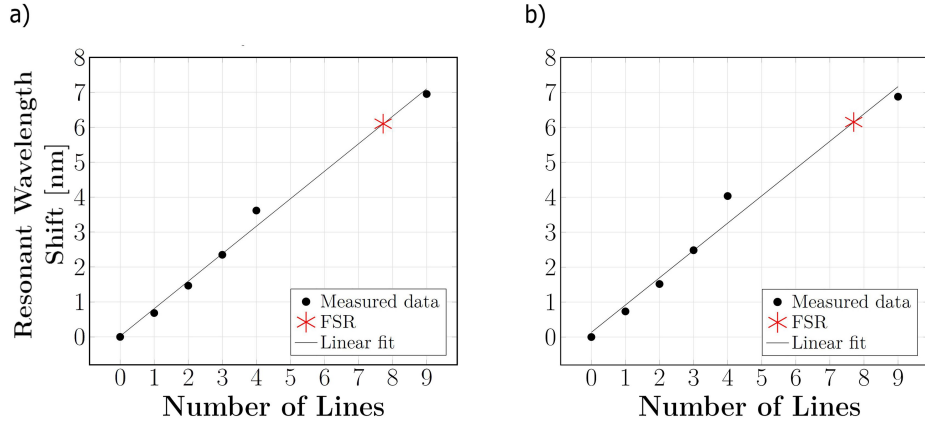

Fig. 5. Dependence of the resonant wavelength shift on the number of lines written across the racetrack. For each line, an arc length of approximately 14 μm has been exposed. a) Device without oxide cladding, b) device with oxide cladding.

L_{exp} is the portion of the total length exposed to the laser), the refractive index of the exposed region (considered uniform across the waveguide) changed by approximately -2×10^{-2}. It is not possible to affirm that this value corresponds to the change in distribution of the refractive index within the waveguide, since the mechanisms of absorption and change in the bond configuration are not fully defined through simulations or measurements. This value is, therefore, given as the average change of the refractive index of the material. In the simulation, the change of the refractive index was homogeneous through the whole thickness of the silicon nitride layer. If the refractive index of the material changed, instead, only near the surface, then the change would have had to be greater to cause the same effect on effective refractive index.

By calculating the Q factor and the extinction ratio of the devices, it was possible to study the effect of exposure on the insertion losses of these devices. The Q factor is around 900 for the
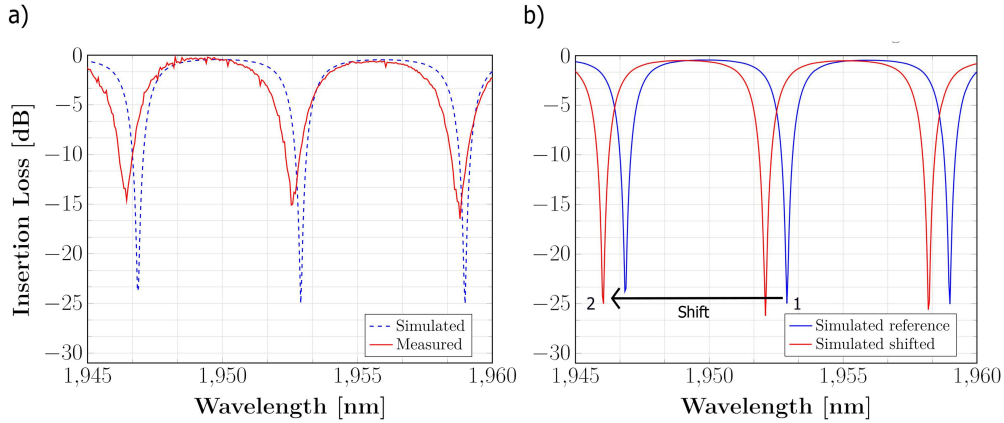
a)

b)

Fig. 6. a) Transmission spectra of the simulated device, compared to the measured spectrum.
b) Transmission spectra obtained by simulation, before and after changing the refractive index of silicon nitride.

device without oxide, and 1100 for the device with oxide on top. The extinction ratio meanwhile, was approximately 11.5 dB in the first case (air cladding), and 12.3 dB in the second case (oxide cladding). Therefore, we concluded that the propagation loss was not significantly affected by the laser trimming procedure. Losses, however, are higher than in the simulation, and both Q factor and extinction ratio are lower compared to the simulation, in particular where the cladding is not present. The insertion loss tends to increase of approximately 0.07 dB after each exposure for the device with oxide cladding, as observable from Figure 4b. This might be due to an added stress in the silicon dioxide layer. The resonant wavelength shift, the Q factor and the extinction ratio are comparable for both chips, both with and without cladding. This is due to the transparency of silicon dioxide at the wavelength of the laser (244 nm).

The mechanisms that lead to the change in the refractive index are still to be investigated. Although, the fact that we obtained the same results, in terms of refractive index, for both chips with and without top oxide cladding, implies that only the silicon nitride is affected by the process. The slight increase in optical losses of the chip cladded with oxide, could also suggest the creation of additional strain as a potential factor in this process. As the nitrogen-rich films used for the devices exhibit a negligible concentration of N-N and Si-Si bonds [13], we believe that the decrease in refractive index is the result of the UV light having enough energy to break the Si-H and, more importantly, the N-H bonds within the film allowing the formation of new Si-N bonds and the release of hydrogen [40, 41]. This effect has been previously observed when SiN films are subjected to thermal annealing and it is often associated with a slight increase of the bandgap of nitrogen-rich films mainly due to the structural rearrangement of the bonding configuration of the Si-N bonds, which results in a smaller refractive index and in the densification of the SiN films [42].

3.3. Temperature stability

The resonant wavelength shift of racetrack resonators is often affected by ambient temperature fluctuations. For this reason, the resonators with and without top oxide cladding have been characterised at different temperatures (in the range of 20 °C to 60 °C). Devices without top oxide cladding experienced a resonant wavelength shift of 22.0 pm/K, while for devices with top oxide cladding a wavelength shift of 23.6 pm/K was measured (see Fig. 7). These values were measured for an interval of wavelengths around 1955 nm. These shifts are, at least, around 30

times smaller than the one observed after the laser writing, suggesting that our results were not strongly affected by the temperature of the environment.
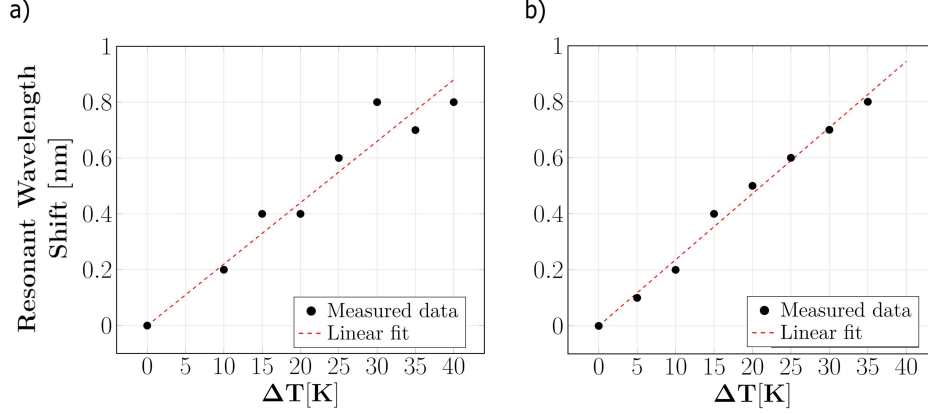
a)

b)

Fig. 7. Measured resonant wavelength shift as a function of change in the ambient temperature. a) device without oxide cladding, and b) device with top oxide cladding.

From the shift of the resonant wavelength with temperature ($d\lambda_r/dT$), the effective thermo-optic coefficient (dn_{eff}/dT) can be calculated using Eq. (1) [43]:

$$\frac{d\lambda_r}{dT} = \frac{\lambda_r}{n_{eff}} \frac{dn_{eff}}{dT} + \lambda_r \alpha_{sub} \tag{1}$$

where $\alpha_{sub} = 2.6 \times 10^{-6}$ K^{-1} is the thermal expansion coefficient of the silicon substrate and λ_r is the resonant wavelength.

The confinement factor relates the effective refractive index with the refractive index of the cladding materials. This relationship is approximately valid also for the derivatives in temperature of the same parameters (effective thermo-optic coefficient and thermo-optic coefficient), and allows to calculate the thermo-optic coefficient of silicon nitride, as explained by Raghunathan *et al.* in [24]. The thermo-optic coefficient of silicon dioxide we considered is equal to 1×10^{-5} K^{-1}. The confinement factor has been derived from simulation of the waveguide, with $n_{SiO2} = 1.44$ and $n_{SiN} = 1.83$, and it is equal to 0.42. The dependence of the confinement factor on the temperature has been neglected, and it has been approximated to a constant value. The resulting thermo-optic coefficient of silicon nitride is 2.23×10^{-5} K^{-1}.

4. Conclusion

For the first time a rapid trimming technique for nitrogen-rich silicon nitride racetrack resonators has been proposed for applications in the mid-IR. From the results obtained, it appears that it is possible to trim repeatedly the operating wavelength of a racetrack resonator by a full FSR and through a non invasive method, which involves the exposure to a UV laser beam. Compared to what has been previously proposed, this technique can be performed in a shorter time frame (a few seconds, compared to many hours) and at room temperature, making it easier to apply in practice and at a lower cost. No additional fabrication step is required for trimming, and the procedure does not need to be carried out in a cleanroom. Since it does not require any additional layer (e.g. a polymer layer), the devices maintain their CMOS compatibility.

Disclosures

The authors declare that there are no conflicts of interest related to this article.

References

1. X. Chen, M. M. Milosevic, S. Stankovic, S. Reynolds, T. Dominguez Bucio, K. Li, D. J. Thomson, F. Y. Gardes, and G. T. Reed, "The Emergence of Silicon Photonics as a Flexible Technology Platform," in *Proceedings of the IEEE,* vol. 106 (2018), pp. 2101–2116.
2. W. Cao, D. Hagan, D. J. Thomson, M. Nedeljkovic, S. U. Alam, J. Wang, F. Y. Gardes, G. T. Reed, G. Z. Mashanovich, C. G. Littlejohns, and M. S. Rouifed, "High-speed Silicon Modulators for the 2 μm Wavelength Band," Optica **5**, 1055–1062 (2018).
3. Z. Li, A. M. Heidt, J. M. O. Daniel, Y. Jung, S. U. Alam, and D. J. Richardson, "Thulium-doped fiber amplifier for optical communications at 2 μm," Opt. Express **21** (2013).
4. G. Z. Mashanovich, M. M. Milosevic, M. Nedeljkovic, N. Owens, B. Xiong, E. J. Teo, and Y. Hu, "Low loss silicon waveguides for the mid-infrared," Opt. Express **19**, 7112 (2011).
5. M. M. Milosevic, M. Nedeljkovic, T. M. Ben Masaud, E. Jaberansary, H. M. Chong, N. G. Emerson, G. T. Reed, and G. Z. Mashanovich, "Silicon waveguides and devices for the mid-infrared," Appl. Phys. Lett. **101**, 1–5 (2012).
6. J. J. Ackert, D. J. Thomson, L. Shen, A. C. Peacock, P. E. Jessop, G. T. Reed, G. Z. Mashanovich, and A. P. Knights, "High-speed detection at two micrometres with monolithic silicon photodiodes," Nat. Photonics **9**, 393–396 (2015).
7. G. T. Reed, G. Z. Mashanovich, F. Y. Gardes, M. Nedeljkovic, Y. Hu, D. J. Thomson, K. Li, P. R. Wilson, S. W. Chen, and S. S. Hsu, "Recent breakthroughs in carrier depletion based silicon optical modulators," Nanophotonics **3**, 229–245 (2014).
8. D. E. Hagan and A. P. Knights, "Mechanisms for optical loss in soi waveguides for mid-infrared wavelengths around 2 μm," J. Opt. **19** (2017).
9. Z. Liu, Y. Chen, Z. Li, B. Kelly, R. Phelan, J. O'Carroll, T. Bradley, J. P. Wooler, N. V. Wheeler, A. M. Heidt, T. Richter, C. Schubert, M. Becker, F. Poletti, M. N. Petrovich, S. ul Alam, D. J. Richardson, and R. Slavík, "High-capacity directly modulated optical transmitter for 2μm spectral region," J. Light. Technol. **33**, 1373–1379 (2015).
10. P. Tai Lin, V. Singh, L. Kimerling, and A. Murthy Agarwal, "Planar silicon nitride mid-infrared devices," Appl. Phys. Lett. **102**, 1–6 (2013).
11. R. Hainberger, P. Muellner, E. Melnik, G. Mutinati, M. Eggeling, A. Maese-novo, F. Vogelbacher, J. Kraft, G. Koppitsch, G. Meinhardt, and F. Schrank, "Silicon Nitride Waveguide Integration Platform for Medical Diagnostic Applications," in *Progress in Electromagnetic Research Symposium (PIERS),* (IEEE, 2016).
12. A. Rahim, E. Ryckeboer, A. Z. Subramanian, B. Kuyken, A. Dhakal, A. Raza, A. Hermans, M. Muneeb, Y. Li, U. Dave, P. Bienstman, and N. L. Thomas, "Expanding the Silicon Photonics Portfolio With Silicon Nitride Photonic Integrated Circuits," J. Light. Technol. **35**, 639–649 (2017).
13. T. Dominguez Bucio, A. Z. Khokhar, C. Lacava, S. Stankovic, G. Z. Mashanovich, P. Petropoulos, and F. Y. Gardes, "Material and optical properties of low- temperature NH 3 -free PECVD SiNx layers for photonic applications," J. Phys. D: Appl. Phys. (2017).
14. T. Dominguez Bucio, C. Lacava, M. Clementi, J. Faneca, I. Skandalos, A. Baldycheva, M. Galli, K. Debnath, P. Petropoulos, and F. Y. Gardes, "Silicon Nitride Photonics for the Near-Infrared," IEEE J. Sel. Top. Quantum Electron. **26**, 1–13 (2020).
15. J. F. Bauters, M. J. R. Heck, D. D. John, S. Jonathon, C. M. Bruinink, A. Leinse, R. G. Heideman, J. Daniel, and J. E. Bowers, "Planar waveguides with less than 0 . 1 dB / m propagation loss fabricated with wafer bonding," Opt. Express **19**, 1272–1278 (2011).

16. Y.-D. Yang, Y. Li, Y.-Z. Huang, and A. W. Poon, "Silicon nitride three-mode division multiplexing and wavelength-division multiplexing using asymmetrical directional couplers and microring resonators," Opt. Express **22**, 22172–22183 (2014).

17. Q. Liu, X. Tu, K. Woo, J. Sheng, Y. Shin, K. Han, Y.-J. Yoon, G.-Q. Lo, and M. Kyoung, "Sensors and Actuators B : Chemical Highly sensitive Mach-Zehnder interferometer biosensor based on silicon nitride slot waveguide," Sensors & Actuators: B. Chem. **188**, 681–688 (2013).

18. Y. Okawachi, K. Saha, J. S. Levy, Y. H. Wen, M. Lipson, and A. L. Gaeta, "Octave-spanning frequency comb generation in a silicon nitride chip," Opt. Lett. **36**, 3398–3400 (2011).

19. A. R. Johnson, A. S. Mayer, A. Klenner, K. Luke, E. S. Lamb, M. R. E. Lamont, C. Joshi, Y. Okawachi, F. W. Wise, M. Lipson, U. Keller, and A. L. Gaeta, "Octave-spanning coherent supercontinuum generation in a silicon nitride waveguide," Opt. Lett. **40**, 5117–5120 (2015).

20. B. E. Little, S. T. Chu, H. A. Haus, J. Foresi, and J. P. Laine, "Microring Resonator Channel Dropping Filters," J. Light. Technol. **15** (1997).

21. Q. Xu, B. Schmidt, S. Pradhan, and M. Lipson, "Micrometre-scale silicon electro-optic modulator," Nature **435**, 325–327 (2005).

22. Y. Sun and X. Fan, "Optical ring resonators for biochemical and chemical sensing," Anal. Bioanal. Chem. pp. 205–211 (2011).

23. M. M. Milosevic, N. G. Emerson, F. Y. Gardes, X. Chen, A. A. D. T. Adikaari, and G. Z. Mashanovich, "Athermal waveguides for optical communication wavelengths," Opt. Lett. **36**, 4659–4661 (2011).

24. V. Raghunathan, W. N. Ye, J. Hu, T. Izuhara, J. Michel, and L. Kimerling, "Athermal operation of Silicon waveguides: spectral, second order and footprint dependencies," Opt. Express **18**, 17631 (2010).

25. M. M. Milosevic, X. Chen, W. Cao, A. F. Runge, Y. Franz, C. G. Littlejohns, S. Mailis, A. C. Peacock, D. J. Thomson, and G. T. Reed, "Ion Implantation in Silicon for Trimming the Operating Wavelength of Ring Resonators," IEEE J. Sel. Top. Quantum Electron. **24**, 1–7 (2018).

26. X. Chen, M. M. Milosevic, D. J. Thomson, A. Z. Khokhar, Y. Franz, A. F. Runge, S. Mailis, A. C. Peacock, and G. T. Reed, "Post-fabrication phase trimming of mach-zehnder interferometers by laser annealing of germanium implanted waveguides," Photonics Res. **5**, 578–582 (2017).

27. B. Chen, X. Yu, X. Chen, M. M. Milosevic, D. J. Thomson, A. Z. Khokhar, S. Saito, O. L. Muskens, and G. T. Reed, "Real-time monitoring and gradient feedback enable accurate trimming of ion-implanted silicon photonic devices," Opt. Express **26**, 24953–24963 (2018).

28. J. J. Ackert, J. K. Doylend, D. F. Logan, P. E. Jessop, R. Vafaei, and A. P. Knights, "Defect-mediated resonance shift of silicon-on- insulator racetrack resonators," Opt. Express **19**, 9431–9435 (2011).

29. D. H. Geuzebroek, E. J. Klein, H. Kelderman, F. S. Tan, D. J. W. Klunder, and A. Driessen, "Thermally Tuneable, Wide FSR Switch based on Micro-ring Resonators," Proc. Symp. IEEE/LEOS Benelux Chapter **1**, 155–158 (2002).

30. J. K. Doylend, D. F. Logan, R. Vafaei, A. P. Knights, L. Chrostowski, J. J. Ackert, and P. E. Jessop, "Defect-mediated resonance shift of silicon-on-insulator racetrack resonators," Opt. Express **19**, 11969 (2011).

31. L. Zhou, K. Okamoto, and S. J. B. Yoo, "Athermalizing and Trimming of Slotted Silicon Microring Resonators With UV-Sensitive PMMA Upper-Cladding," IEEE Photonics Technol. Lett. **21**, 1175–1177 (2009).

32. D. K. Sparacin, C.-Y. Hong, L. C. Kimerling, J. Michel, J. P. Lock, and K. K. Gleason, "Trimming of microring resonators by photo-oxidation of a plasma-polymerized organosilane cladding material," Opt. Lett. **30**, 2251–2253 (2005).

33. D. K. Sparacin, J. P. Lock, C.-y. Hong, K. K. Gleason, L. C. Kimerling, and J. Michel, "Trimming of Silicon Nitride Microring Resonators with a Polysilane Top Cladding," IEEE Int. Conf. on Group IV Photonics **1**, 117–119 (2005).

34. J. Schrauwen, D. V. Thourhout, and R. Baets, "Trimming of silicon ring resonator by electron beam induced compaction and strain," Opt. Express **16**, 135–137 (2008).

35. S. Ueno, T. Naganawa, and Y. Kokubun, "High UV sensitivity of SiON film and its application to center wavelength trimming of microring resonator filter," IEICE Transactions on Electron. **E88-C**, 998–1004 (2005).

36. H. Haeiwa, T. Naganawa, and Y. Kokubun, "Wide Range Center Wavelength Trimming of Vertically Coupled Microring Resonator Filter by Direct UV Irradiation to SiN Ring Core," IEEE Photonics Technol. Lett. **16**, 135–137 (2004).

37. S. L. Scholl, A. Jantzen, R. H. S. Bannerman, P. C. Gow, D. H. Smith, J. C. Gates, L. J. Boyd, P. G. R. Smith, and C. Holmes, "Thermal approach to classifying sequentially written fiber Bragg gratings," Opt. Lett. **44**, 703 (2019).

38. C. Holmes, P. A. Cooper, H. N. J. Fernando, A. Stroll, J. C. Gates, C. Krishnan, R. Haynes, P. L. Mennea, L. G. Carpenter, C. B. E. Gawith, M. M. Roth, M. D. Charlton, and P. G. R. Smith, "Direct uv written planar bragg gratings that feature zero fluence induced birefringence," Meas. Sci. Technol. **26**, 125006 (2015).

39. C. Holmes, J. C. Gates, L. G. Carpenter, H. L. Rogers, R. M. Parker, P. A. Cooper, S. Chaotan, F. R. M. Adikan, C. B. E. Gawith, and P. G. R. Smith, "Direct UV-written planar bragg grating sensors," Meas. Sci. Technol. **26**, 112001 (2015).

40. J. J. Mei, H. Chen, W. Z. Shen, and H. F. Dekkers, "Optical properties and local bonding configurations of hydrogenated amorphous silicon nitride thin films," J. Appl. Phys. **100** (2006).

41. I. Parkhomenko, L. Vlasukova, F. Komarov, O. Milchanin, M. Makhavikou, A. Mudryi, V. Zhivulko, J. Żuk, P. Kopyciński, and D. Murzalinov, "Origin of visible photoluminescence from Si-rich and N-rich silicon nitride films," Thin Solid Films **626**, 70–75 (2017).

42. H. Charifi, A. Slaoui, J. P. Stoquert, H. Chaib, and A. Hannour, "Opto-structural properties of silicon nitride thin films deposited by ecr-pecvd," World J. Condens. Matter Phys. **6**, 7–16 (2016).
43. J. Teng, P. Dumon, W. Bogaerts, H. Zhang, X. Jian, M. Zhao, G. Morthier, and R. Baets, "Athermal SOI ring resonators by overlaying a polymer cladding on narrowed waveguides," IEEE Int. Conf. on Group IV Photonics GFP pp. 77–79 (2009).